Electrocatalytic performance SiO_2-SWCNT nanocomposites prepared by electroassisted deposition

Alonso Gamero-Quijano[1], Francisco Huerta[2], David Salinas-Torres[1], Emilia Morallón[1,], Francisco Montilla[1,*]*

[1]Dept. Química Física e Instituto Universitario de Materiales, Universidad de Alicante, Ap. 99, E-03080, Alicante, Spain. [2]Dept. Ingenieria Textil y Papelera, Universitat Politecnica de Valencia, Plaza Ferrandiz y Carbonell, 1. E-03801, Alcoy, Spain

Abstract

Composite materials made of porous SiO_2 matrices filled with single-walled carbon nanotubes (SWCNT) were deposited on electrodes by an electro-assisted deposition method. The synthesized materials were characterized by several techniques, showing that porous silica prevents the aggregation of SWCNT on the electrodes, as could be observed by TEM microscopy and Raman spectroscopy. Different redox probes were employed to test their electrochemical sensing properties. The silica layer allows the permeation of the redox probes to the electrode surface and improves the electrochemical reversibility indicating an electrocatalytic effect by the incorporation of dispersed SWCNT onto the silica films.

Keywords: Silica modified electrodes, sol-gel, SWCNT modified electrodes, nanostructured sensors, electro-assisted deposition, dopamine sensing

*Corresponding author: francisco.montilla@ua.es; morallon@ua.es

1. Introduction

The detection and measurement of extremely small amounts of molecules of biological interest is a recent challenge in chemical analysis and biomedicine. The need for smaller, faster, and simpler sensors for molecular analysis has stimulated the development of new electrocatalytic materials and therefore of new electrochemical devices [1;2]. In this evolution process, the size of the working materials reached soon the nanometer scale (thin films, nanoparticles, nanotubes, graphene, etc.), approaching the size of the target molecules [2-5]. This point is of significant interest because most of the nanomaterials exhibit novel electronic, optical or mechanical properties, which are inherent to the nanoscale dimension.

Most of nanomaterials are isotropic, however single-walled carbon nanotubes (SWCNT) can be considered as one-dimensional structures because of their large length-to-width ratio. Besides, they constitute an interesting group of materials in electrocatalysis due to their outstanding results as sensing elements. Electrodes modified with carbon nanotubes have been applied to the electroanalytical determination of a great amount of species (tyrosine, insulin, quercetin, dopamine, uric acid, NADH, among others) [6-11] and have been used as transducers for direct electron transfer to redox enzymes [12;13].

However, carbon nanotubes show strong tendency to aggregation when they are deposited on the substrate (as a result of the strong π-π attractive interaction between the tube walls). It results in a limited sensibility of the electrochemical devices [14]. This is a common problem shared by most of the electrodes modified with nanomaterials [15-19].

When the aggregation takes place, some of the physicochemical properties, which appeared thanks to the nanostructured character of the material, are usually lost in the macroscopic measurement. A clear example of that was presented in our previous work in

which glassy carbon electrodes were modified with SWCNT. Those electrodes presented enhanced electrocatalytic performance for several redox probes (such as dopamine, ascorbic acid, quinones and Fe^{3+}/Fe^{2+}) [20]. However, despite the significant enlargement of the heterogeneous electron transfer rate observed, in most cases less than 1% of the electrode surface was actually transferring charge to species in solution. Such a low value revealed that most carbon nanotubes were aggregated and therefore, that the surface corresponding to the carbon nanotube walls was blocked.

Hence, achieving a real dispersion of the active material onto the supporting electrode is a key point in the field of nanostructured sensors. A simple way could be the immobilization of the material inside a porous inorganic matrix. Some reports show how carbon nanotubes or nanoparticles can be dispersed in mesoporous SiO_2 structures obtained by either chemical vapor deposition [21-23] or sol-gel methods [24-28].

In previous studies, we showed that the pores of an electrochemically deposited SiO_2 matrix could be filled with a conducting polymer like polyaniline [29;30]. Such a result opened up the possibility of producing other hybrid SiO_2-based nanostructures with a conductive character and therefore appropriate for electrochemical applications.

The present work shows the preparation of silica matrices filled with single-walled carbon nanotubes (SWCNT) in a single electrochemical step on glassy carbon substrates. Raman spectroscopy, imaging techniques and electrochemical methods have been used to characterize the obtained material. The modified electrodes have been applied to the electrochemical sensing of standard redox probes.

2. Experimental part

2.1. Reagents and equipment

SWCNT were purchased from Cheap Tubes Inc. (Brattleboro, VT, USA) with a purity of 95% and 1-2 nm of diameter. SWCNT were used without further purification. Tetraethyl orthosilicate (TEOS) (Sigma-Aldrich), iron (II) sulfate heptahydrate (Merck, p.a.), Potassium chloride (Merck, p.a.), iron (III) sulfate hydrate (Panreac, p.a.), dopamine (DA, Sigma-Aldrich p.a.), poly(4-styrenesulfonic acid) 18% wt. (PSS, Sigma-Aldrich), hydrochloric acid (Merck, p.a.) and sulfuric acid (Merck, p.a.) were also used as received. All solutions were prepared with purified water obtained from an Elga Labwater Purelab system (18.2 MΩ cm).

Electrochemical experiments were performed in conventional electrochemical glass cells. The working electrode was a glassy carbon bar (GC, Carbone Lorraine). The working electrode GC was carefully polished with fine emery paper and diamond suspension (Buehler, 1µm and 0.25 µm) over cloth and then ultrasonically cleaned in distilled water. A platinum wire was employed as counter electrode, and a reversible hydrogen electrode (RHE) introduced in the same electrolyte solution placed in a Luggin capillary was used as reference electrode.

Cyclic voltammograms were performed with an Autolab PGSTAT30 equipped with a SCAN-GEN module. The current density was calculated from the geometric area of the electrode. The surface morphology of the electrodes was studied by scanning electron microscopy (SEM JEOL JSM-840) and transmission electron microscopy (TEM JEOL model JEM-2010). The scanning electron microscopy was performed directly on the working electrode of glassy carbon. For transmission electron microscopy studies, the

electrodeposited silica samples were carefully scratched from the surface of the glassy carbon electrode. This silica powder was dried by vacuum heating at 40°C, subsequently dispersed with ethanol and dosed over the sample holder. Confocal Raman spectra were collected with a FT-Raman (Bruker RFS/100) model using a Nd-YAG laser source (1064 nm).

Porous texture was characterized by physical adsorption of N_2 (-196 ºC) and CO_2 (0 ºC), using an automatic adsorption system (Autosorb-6, Quantrachrome). The samples were outgassed at 150 °C under vacuum for 4 h. Nitrogen adsorption results were used to determine BET surface area values and Dubinin-Radushkevich (DR) micropore volumes (V_{DR} N_2) as well as the average pore size. Narrow micropore volume (pore size < 0.7 nm, approximately) was obtained from CO_2 adsorption data (V_{DR} CO_2).

2.2. Preparation of SWCNT@SiO_2 modified electrodes

The carbon nanotubes were encapsulated in pure silica matrices, during its deposition on glassy carbon electrodes. Initially, 2 stock solutions were prepared following the next procedure:

Solution 1: Stable SWCNT aqueous suspensions were obtained as follows, 100 mg of SWCNT were poured into a vial containing 20 ml of 1% poly(4-styrenesulfonic acid) aqueous solution. This mixture was stirred with an ultrasonic probe VIRTIS (Virsonic 475, 475W maximum output power) at 1 minute intervals for 1h. To avoid overheating, samples were air-cooled between sonication intervals. This suspension is stable for several months, due to the formation of SWCNT-PSS assemblies, as described by Dobbins and co-workers [31].

Solution 2: Silica stock solution was prepared through the alcohol-free sol-gel route [32;33]. 1.00 mL of TEOS was mixed under vigorous stirring with 2.52 mL of a 0.46M KCl+0.01M HCl solution in a closed vessel. After 2 hours, the resulting sol was submitted to evaporation by vacuum heating until the complete removal of the released ethanol coming from alkoxyde hydrolysis.

For the modification of glassy carbon electrodes 2.52 mL of solution **1** –SWCNT suspension– was poured into solution **2** –alcohol-free silica precursor–. Achieving the complete removal of ethanol from the silica precursor solution is a key point, since the SWCNT-PSS assemblies are unstable in the presence of alcohol.

This mixture containing SWCNT and the hydrolyzed silica precursor was placed in an electrochemical glass cell, which contained a platinum wire counter electrode and a reversible hydrogen reference electrode.

The deposition of silica was performed potentiostatically by the immersion of a polished GC working electrode in the precursor solution, where was pre-conditioned at a constant potential of 0.0 V and then stepped down to –1.2V for 60 seconds to trigger the deposition of the silica film. Hydrogen evolution upon electrochemical reduction of water at this potential leads to a pH rise in the electrode surroundings. This induces the collapse of silica colloids near the electrode surface and favours their deposition. As a result, the silica film traps the suspended SWCNT to form the material called SWCNT@SiO_2. Further details on the deposition method are given elsewhere [30].

The amount of nanotubes incorporated into the silica matrices was estimated by thermogravimetric analysis. The silica samples were subjected to thermal treatment at 10ºC/min up to 900 ºC in 100 ml/min of nitrogen/oxygen flow (ratio: 4/1). The mass

fraction of SWCNT as determined by TG resulted in a value of nearly 0.2 wt% in the silica-PSS layer.

3. Results and discussion

3.1. Characterization of SWCNT@SiO_2 composites

Figure 1 shows SEM micrographs obtained from a bare glassy carbon electrode and the same electrode after the electrochemically assisted deposition of the SWCNT@SiO_2 composite.

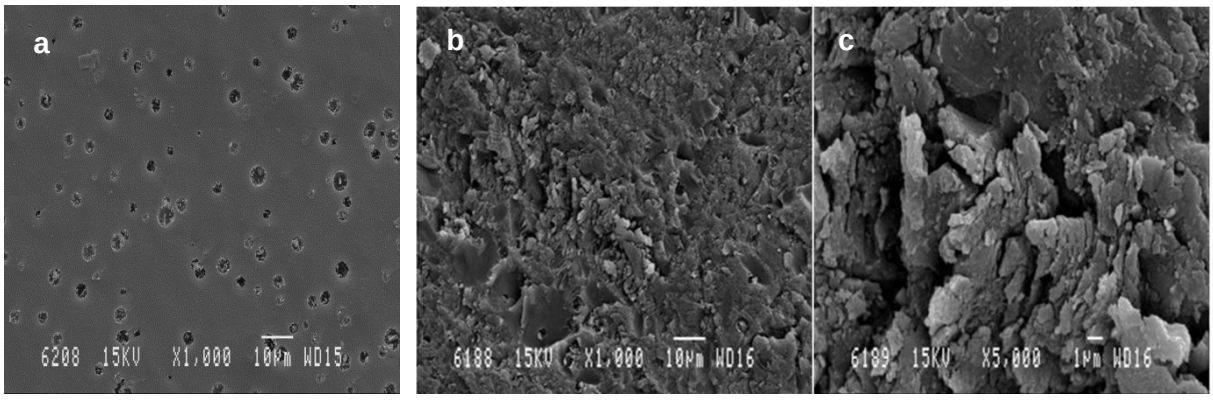

Figure 1: SEM micrographs acquired at different magnifications from: a) bare glassy carbon electrode, b) and c) glassy carbon substrate after the electroassisted deposition of the SWCNT@SiO_2 composite.

The surface morphology of the silica-encapsulated SWCNT looks very rough compared with bare glassy carbon substrate, although SWCNT structures cannot be detected at these magnifications. Both images contrast with the surface morphology observed for a SWCNT-modified glassy carbon electrode prepared by drop-casting from DMF suspensions. In that case, the morphology was characterized by the presence of carbon nanotube aggregates

with diameters ranging between 30 and 80 nm. It was attributed to the presence of nanotube bundles formed by 200–1600 units [20].

In contrast, the images of figure 1 are compatible with a better SWCNT dispersion after the electrochemically assisted deposition. Obviously, the presence of SWCNT encapsulated within the silica film must be confirmed by additional techniques, as TEM microscopy or Raman spectroscopy.

Transmission electron microscopy seems more appropriate to observe the inner structure of the silica matrix and, hence, to check the eventual incorporation of carbon nanotubes. TEM images recorded from the SWCNT@SiO_2 deposit are presented in figure 2 at different magnifications.

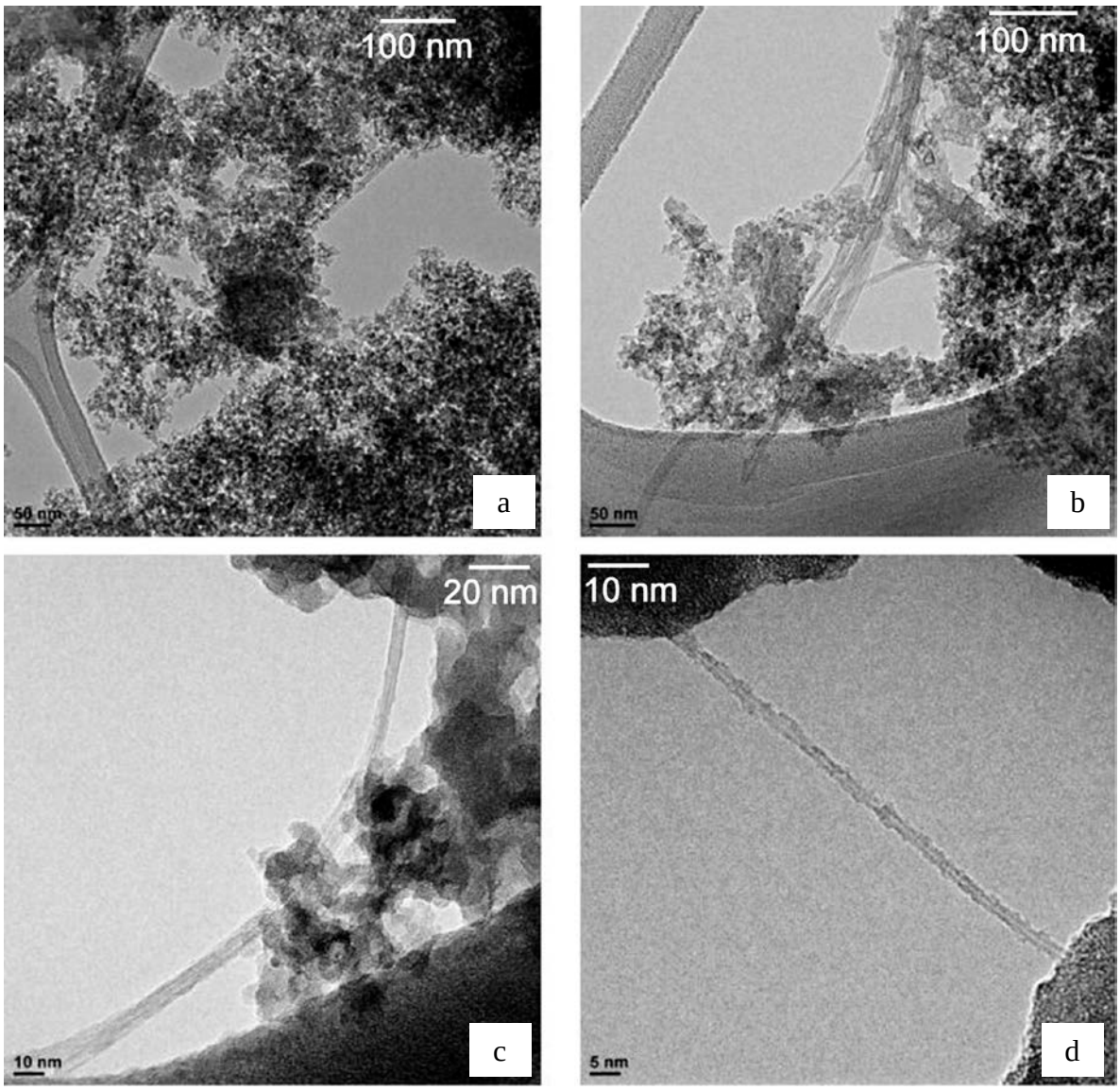

Figure 2. TEM micrographs of SWCNT@SiO_2 composites prepared by electroassisted deposition. (a) General view of the SWCNT@SiO_2 composite; (b) and (c) details of nanotubes bundles; (d) isolated SWNT found in-between SiO_2 aggregates.

The silica deposits are characterized by its globular aspect, which is due to the electrochemically assisted deposition of silica colloids. Some SWCNT aggregates can be observed in Fig 2b and 2c. These aggregates comprise around 3-10 SWCNT, and in some cases, isolated single-walled carbon nanotubes can be observed, as in Fig. 2d. These images

prove that SWCNT can be effectively incorporated and isolated within the porous silica matrix.

Nitrogen adsorption isotherms of dryed silica samples reveal that the materials are essencially microporous with an average pore size of about 1.5 nm (Table 1). This value of the hydrated silica cannot be obtained via this technique. However, it should be significantly larger in the hydrogel than in dry samples and hence higher than the size of redox probes used in the voltammetric experiments.

Table 1. Calculated BET surface area (S_{BET}) and pore volume (V) using DR model on either N_2 or CO_2 isotherms for the SiO_2-PSS.

Sample	**S_{BET} (m^2 g^{-1})**	**$V_{DR(N2)}$ (cm^3 g^{-1})**	**$V_{DR(CO2)}$ (cm^3 g^{-1})**
SiO_2-PSS	445	0.22	0.22

Raman spectroscopy has become an important tool in the characterization of carbon materials because this technique is particularly sensitive to the microstructure of the carbon. The Raman response of these materials results from the scattering of light from carbon lattice phonons. So, additional evidences on the incorporation and aggregation state of SWCNT into SiO_2 are expected from Raman spectroscopy experiments.

Fig. 3 shows two set of spectra recorded in different frequency regions from the bare glassy carbon substrate (GC), carbon nanotubes deposited on glassy carbon from DMF

solutions (SWCNT) and carbon nanotubes electrochemically incorporated into the silica structure (SWCNT@SiO_2).

The spectrum of GC is characterized by the presence of bands at 1331, 1592 and 2652 cm^{-1}. The former band is known as D-band and it is originated from the A_{1g} in-plane breathing vibration and corresponds to disordered sp^2 bonds or defects. The band at 1592 cm^{-1}, G-band or graphite tangential band arises from the E_{2g} in-plane vibration and comes from carbon atoms showing sp^2 hybridization and planar configuration. Finally, the high-energy band around 2600 cm^{-1} corresponds to an overtone of the D-band.

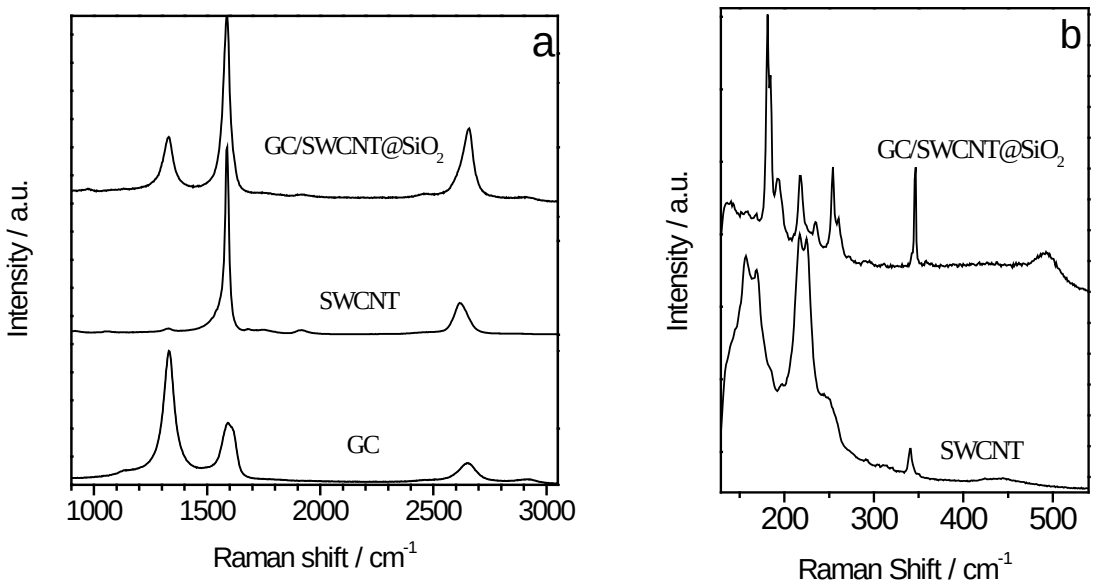

Figure 3: Raman spectra recorded (a) in the full frequency range and (b) RBM frequency region for: Bare glassy carbon electrode (labelled as GC), SWCNT powder from a DMF suspension (labelled as SWCNT) and SWCNT@SiO_2 prepared by electroassisted deposition deposited on a GC electrode (labelled as GC/SWCNT@SiO_2).

The intensity ratio of the former two bands (I_D/I_G) is considered as a parameter to assess the degree of disorder of the sample. The spectrum of the bare glassy carbon substrate is characterized by the high relative intensity of the feature assigned to disordered carbon species. On the contrary, D-band vanishes when SWCNT powder is deposited on a GC electrode, and the spectrum is dominated by the G-band, which reveals the presence of well-ordered sp^2 carbon domains. Fig. 3(a) shows, for the GC/SiO_2-SWCNT electrode, both G and D bands sample. It should be noted that the relative intensity of the G band is significantly higher than in the case of the bare GC spectrum. From this observation, it is confirmed the presence of highly ordered carbon species, which supports the incorporation of SWCNT into the silica matrix.

An additional proof on the presence and aggregation state of the SWCNT at silica is obtained from the examination of the low-energy Raman spectrum in fig. 3b. That spectral region corresponds to the *Radial Breathing Modes* (RBM) of carbon nanotubes. As expected, bare GC do not show active modes in this frequency range (spectrum not shown), but the presence of RBM bands in the other two samples proves the incorporation of carbon nanotubes to the SiO_2 host matrix.

The RBM features are extremely sensitive to the presence of aggregated carbon nanotubes. The spectrum of the SWCNT prepared from DMF suspensions are characterized by the presence of two main convoluted bands at wavelengths (around 160 and 220 cm^{-1}). It has been shown by O'Connell et al [34] that bundling effects produce red shifting of the RBM frequency, compared with the spectra of isolated nanotubes.

The spectrum of the GC/SWCNT@SiO_2 sample presents several well-defined and narrow bands at 180, 193, 218, 236, 254 and 347 cm^{-1}. Assuming that these modes correspond to individual nanotubes (according to the above TEM results the assumption is feasible) the recorded frequencies can be related with diameters ranging between 0.73 and 1.44 nm [35;36]. The higher energies of those vibrations indicate that SWCNT present a better dispersion than the previous sample. The results obtained from both spectroscopic and microscopic techniques reveal that SWCNT are properly incorporated, and well dispersed within the silica porous matrix.

3.2. Analysis of the electrochemical performance of SWCNT@SiO_2-modified electrodes

An organic (dopamine) and an inorganic (Fe^{2+}/Fe^{3+} couple) standard redox probes have been employed to study the electrochemical properties of SWCNT@SiO_2-modified electrodes. Those redox probes were chosen for the evaluation of electron transfer kinetics from the different carbon electroactive sites. The Fe^{2+}/Fe^{3+} redox couple is strongly electrocatalyzed at oxidized carbon surfaces [37]. This redox system is particularly sensitive to the presence of the surface oxygen groups, specifically to the presence of carbonyl species on the carbon surface, which happens mainly in the nanotubes tips [38]. Dopamine redox probe is characterized by the specific adsorption of the quinone-like species on basal planes of the carbon electrodes, i.e. nanotube walls [37].

Fig. 4a shows the stabilized voltammograms recorded in 10 mM iron (II) sulfate / iron (III) sulfate solution for bare glassy carbon electrodes or covered with the SWCNT@SiO_2 composite.

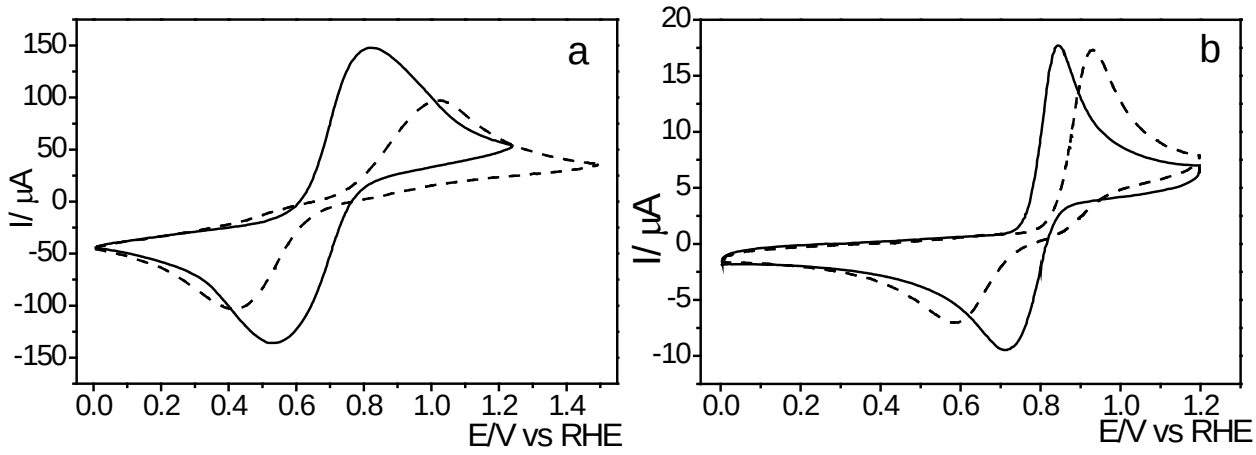

Figure 4: Stabilized cyclic voltammograms of glassy carbon electrodes (GC, dashed lines) or glassy carbon electrodes modified with single walled carbon nanotubes incorporated into silica layers (GC/SWCNT@SiO_2, solid lines). Test solutions: **(a)** 0.5 M H_2SO_4 + 10 mM iron (II) sulfate/ 10 mM iron (III) sulfate solution and **(b)**: 0.5 M H_2SO_4 + 1mM dopamine solution; scan rate: 50 mV/s; electrode geometric area: 0.07 cm^2.

For the GC electrode, an anodic peak appears at 1.03 V reflecting the Fe^{2+} to Fe^{3+} oxidation (E_{ox}) during the positive-going potential sweep. In the reverse scan the faradaic counter-process takes place and a reduction peak is recorded at E_{red}= 0.42 V.

For the GC/SWCNT@SiO_2 electrode, the oxidation peak appears shifted to lower values (E_{ox}=0.82V). The same electrocatalytic effect can be observed for the cathodic process, which is shifted to more positive potentials (E_{red}=0.52V). The peak separation drops from 610 mV, for the bare GC electrode, down to 300 mV in the presence of SWCNT.

Fig. 4b shows the stabilized cyclic voltammogram for the dopamine probe. The oxidation peak for dopamine on the GC electrode appears at 0.93V in the forward scan, whereas the counter-process (dopaminequinone reduction) takes place with a reduction peak centered at

0.58V in the backward sweep, peak separation amounts to 350 mV for the bare GC electrode.

Strong electrocatalytic effect is observed for both anodic and cathodic processes after the modification of the electrode with SWCNT@SiO_2. The oxidation peak shifts to 0.84V and the reduction peak moves to 0.71V, which yields a peak separation of 130 mV.

The electrocatalytic effect observed can be quantified by the calculation of the heterogeneous transfer rate constant $K°$ (cm s^{-1}). From the voltammetric peak-to-peak separations obtained at different scan rates, a value for $K°$ can be obtained by applying the Nicholson's method. More details on the procedure for this analysis can be found in our previous paper [20].

Figure 5 shows stabilized cyclic voltammograms of GC and GC/SWCNT@SiO_2 electrodes recorded at various scan rates in the test solutions. As expected, both the oxidation and the reduction currents raise as the scan rate is increased. The peak separation becomes higher as higher the scan rate, which reveals the quasireversible character of the redox processes involved.

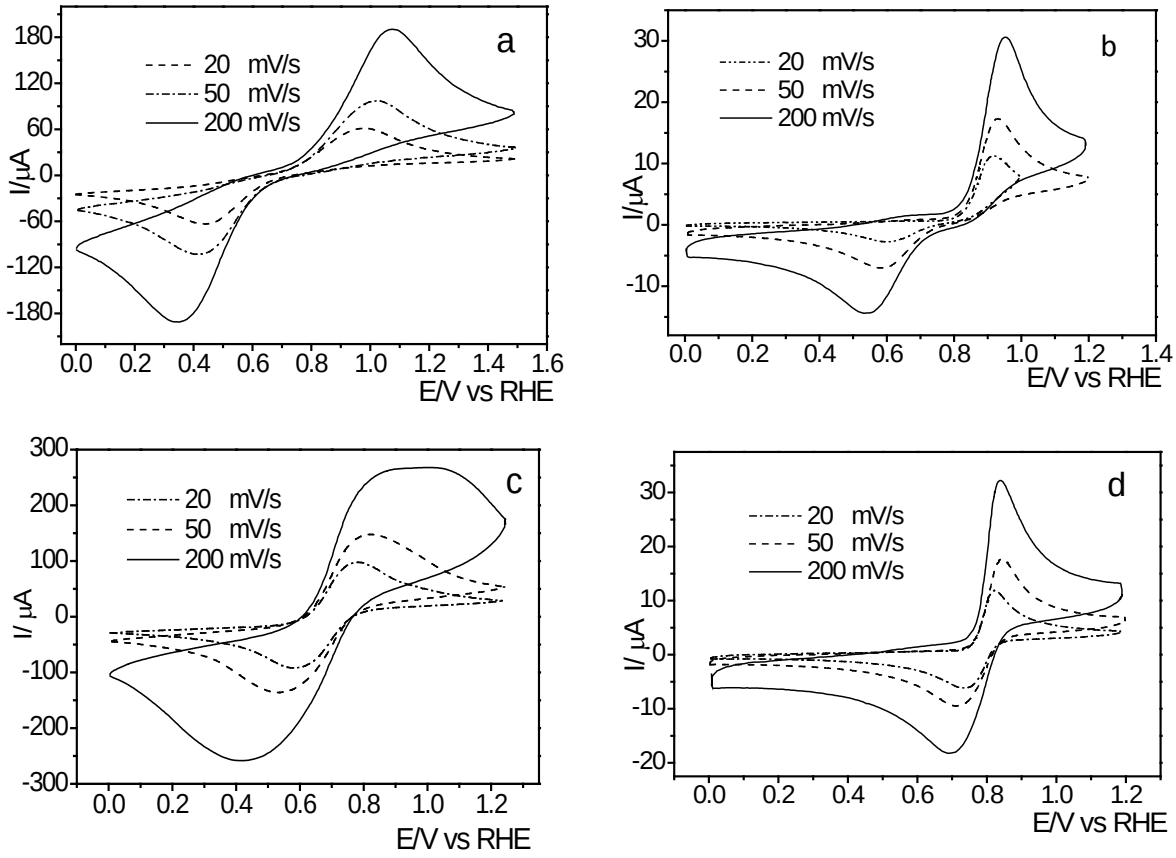

Figure 5: Steady state cyclic voltammograms recorded at different scan rates for: a) GC in 0.5 M H_2SO_4 + 10 mM iron (II) sulfate/ 10 mM iron (III) sulfate solution; b) GC in 0.5 M H_2SO_4 + 1 mM dopamine solution. c) GC/SWCNT@SiO_2 in 0.5 M H_2SO_4 + 10 mM iron (II) sulfate/ 10 mM iron (III) sulfate solution; d) GC/SWCNT@SiO_2 in 0.5 M H_2SO_4+ 1 mM dopamine solution. Electrode geometric area: 0.07 cm^2 in all cases.

Table 2 shows the peak separations, ΔE_p, and corresponding $K°$ values calculated for the redox probes. The obtained $K°$ values on the bare glassy carbon electrodes were 4.9 $x10^{-6}$ cm s^{-1} for dopamine and 1.1 $x10^{-5}$ cm s^{-1} for Fe^{2+}/Fe^{3+} system. After the chemical modification of GC with SWCNT, the transfer rate constant increases significantly in more than one order of magnitude for both redox probes.

Table 2. Values for the voltammetric peak separation (ΔE_p) at 50 mV s^{-1} and heterogeneous transfer rate constant ($K°$) for dopamine and Fe^{2+}/Fe^{3+} redox probes

Redox Probe	Electrode	ΔE_p (mV)	$K°$ ($cm \cdot s^{-1}$)
Fe^{2+}/Fe^{3+}	GC	610	1.1×10^{-5}
	GC/SWCNT@SiO_2	300	2.4×10^{-4}
Dopamine	GC	350	4.9×10^{-6}
	GC/SWCNT@SiO_2	130	5.9×10^{-4}

A similar improvement of the transfer rate was already observed in our previous studies, where GC electrode surface were modified SWCNT deposited from a DMF suspension [20]. The methodology for the SWCNT deposition presented here provides much higher dispersion of SWCNT on the electrode surface than in the previous study. In other words, a similar electrocatalytic efficiency is obtained with much less quantity of carbon nanotubes deposited.

Another physicochemical factor of particular interest in electrocatalysis is the so-called *electroactive area*. Obviously, the electroactive area of an electrocatalyst is related with its geometric area. As a result, the higher the exposed surface, the higher currents recorded across the electrode-solution interface. Nevertheless, the true significance of the electroactive area is that reveals which portion of surface remains available for the transfer of charge to species in solution. In other words, it measures the efficiency of the exposed surface to the electrocatalytic reaction.

The electroactive area can be estimated by the Randles-Sevcik equation [39], which relates the peak current, I_P, with the square root of the scan rate. A linear plot means that the process is controlled by the electron transfer as follows:

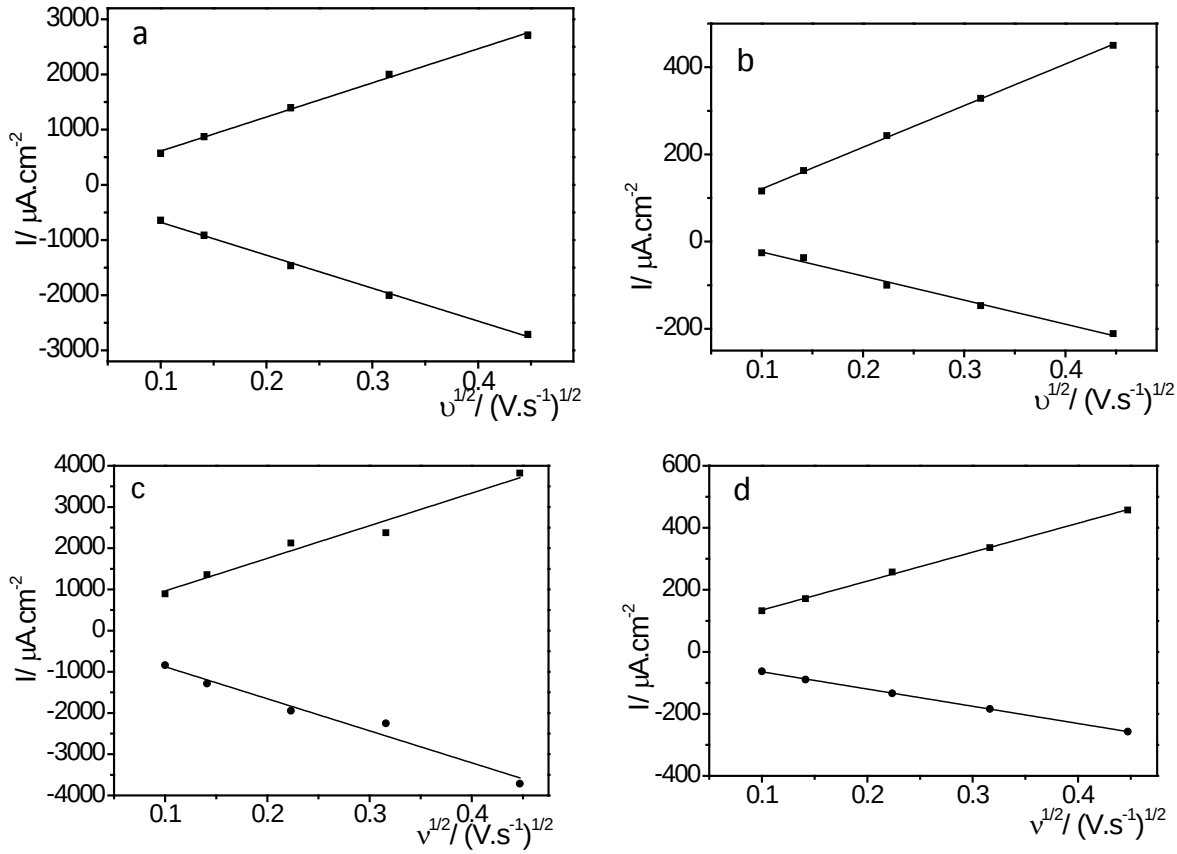

Figure 6: Randles-Sevcik plots obtained from voltammetric data for: a) GC in 10 mM Fe^{2+}/Fe^{3+} solution; b) GC in 1 mM dopamine solution; c) GC/ SWCNT@SiO_2 in 10 mM Fe^{2+}/Fe^{3+} solution; d) GC/SWCNT@SiO_2 in 1 mM dopamine solution. Electrode geometric area: 0.07 cm^2 in all cases.

Table 3: Electroactive area for the electron transfer derived from the Randles-Sevcik equation for Fe^{2+}/Fe^{3+} and dopamine redox probes.

Redox probe	Electrode	Randles-Sevcik slope	Electroactive Area (cm^2)
Fe^{2+}/Fe^{3+}	GC	4.33×10^{-4}	0.066
	GC/SWCNT@SiO_2	5.54×10^{-4}	0.084
Dopamine	GC	6.69×10^{-5}	0.034
	GC/SWCNT@SiO_2	6.54×10^{-5}	0.033

4. Conclusions

The present work shows the synthesis of silica matrices filled with SWCNT. The composite material was prepared on glassy carbon substrates by an electroassisted-deposition method. TEM images and Raman spectroscopy results show that the electroassisted deposition constitutes an effective way to achieve high dispersions of SWCNT within porous layers of SiO_2.

The electrochemical properties of the SWCNT@SiO_2 composite material were tested against either organic (dopamine) or inorganic (Fe^{3+}/Fe^{2+}) redox probes. Thanks to its porous structure, the silica layer allows the permeation of the redox probes to the electrode surface. The improved reversibility for the redox probes studied is due to the electrocatalytic effect provided by the SWCNT dispersed within the silica matrix.

The value of electroactive area, which measures the efficiency of the exposed surface to the catalytic reaction, rises after dispersion of SWCNT in SiO_2. However, the obtained figures are still far from their theoretical maxima, probably showing that a significant number of nanotubes, being accessible, remain electrically isolated from the electrode surface.

This work shows that the electroassisted deposition of silica is a suitable technique to deposit dispersed nanotubes. Generally, nanostructured materials such as graphene, nanoparticles, nanotubes or quantum dots, among others, present a strong tendency to aggregation causing a significant loss of their special properties when deposited on a solid substrate. The results shown in this work make the electro-assisted deposition a feasible way to prevent aggregation and to improve the electrocatalytic performance of nanostructured catalysts.

5. Acknowledgements

This work was financed by the following research projects: MAT2010-15273 of the Spanish *Ministerio de Economia y Competitividad* and FEDER, PROMETEO/2013/038 of the GV and CIVP16A1821 of the *Fundación Ramón Areces*. Alonso Gamero-Quijano acknowledges to *Generalitat Valenciana* the funding of his research fellowship (*Santiago Grisolia Program*). David Salinas-Torres acknowledges to *Ministerio de Economia y Competitividad* the funding of his research fellowship.

Reference List

1. P. Alivisatos, *Nature Biotechnology*, 2004**, 22**, 47.
2. S. Stankovich, D. A. Dikin, G. H. Dommett, K. M. Kohlhaas, E. J. Zimney, E. A. Stach, R. D. Piner, S. T. Nguyen, and R. S. Ruoff, *Nature*, 2006**, 442**, 282.
3. D. W. Schaefer and R. S. Justice, *Macromolecules*, 2007**, 40**, 8501.
4. M. Endo, M. S. Strano, and P. M. Ajayan, *Carbon Nanotubes*, 2008**, 111**, 13.
5. C. E. Banks and R. G. Compton, *Analyst*, 2006**, 131**, 15.
6. R. H. Baughman, A. A. Zakhidov, and W. A. de Heer, *Science*, 2002**, 297**, 787.
7. Y. H. Lin, F. Lu, Y. Tu, and Z. F. Ren, *Nano Letters*, 2004**, 4**, 191.
8. B. R. Azamian, J. J. Davis, K. S. Coleman, C. B. Bagshaw, and M. L. H. Green, *Journal of the American Chemical Society*, 2002**, 124**, 12664.
9. W. Yang, K. Ratinac, S. Ringer, P. Thordarson, J. Γ. Gooding, and F. Braet, *Angewandte Chemie International Edition*, 2010**, 49**, 2114.
10. C. E. Banks and R. G. Compton, *Analyst*, 2005**, 130**, 1232.

11. L. Mazurenko, M. Etienne, O. Tananaiko, V. Zaitsev, and A. Walcarius, *Electrochimica Acta*, 2012**, 83**, 359.

12. J. M. P. Paloma Yáñez-Sedeño, J. Riu, and F. X. Rius, *TrAC Trends in Analytical Chemistry*, 2010**, 29**, 939.

13. Z. J. Wang, M. Etienne, S. Poller, W. Schuhmann, G. W. Kohring, V. Mamane, and A. Walcarius, *Electroanalysis*, 2012**, 24**, 376.

14. R. Bandyopadhyaya, E. Nativ-Roth, O. Regev, and R. Yerushalmi-Rozen, *Nano Letters*, 2002**, 2**, 25.

15. C. Park, Z. Ounaies, K. A. Watson, R. E. Crooks, J. Smith, S. E. Lowther, J. W. Connell, E. J. Siochi, J. S. Harrison, and T. L. S. Clair, *Chemical Physics Letters*, 2002**, 364**, 303.

16. O. Matarredona, H. Rhoads, Z. R. Li, J. H. Harwell, L. Balzano, and D. E. Resasco, *Journal of Physical Chemistry B*, 2003**, 107**, 13357.

17. L. Vaisman, H. Wagner, and G. Marom, *Advances in Colloid and Interface Science*, 2006**, 128**, 37.

18. Y. C. Xing, *Journal of Physical Chemistry B*, 2004**, 108**, 19255.

19. J. J. Liang, Y. Huang, L. Zhang, Y. Wang, Y. F. Ma, T. Y. Guo, and Y. S. Chen, *Advanced Functional Materials*, 2009**, 19**, 2297.

20. D. Salinas-Torres, F. Huerta, F. Montilla, and E. Morallón, *Electrochimica Acta*, 2011**, 56**, 2464.

21. Z. F. Ren, Z. P. Huang, J. W. Xu, J. H. Wang, P. Bush, M. P. Siegal, and P. N. Provencio, *Science*, 1998**, 282**, 1105.

22. W. Z. Li, S. S. Xie, L. X. Qian, B. H. Chang, B. S. Zou, W. Y. Zhou, R. A. Zhao, and G. Wang, *Science*, 1996**, 274**, 1701.

23. M. Terrones, N. Grobert, J. Olivares, J. P. Zhang, H. Terrones, K. Kordatos, W. K. Hsu, J. P. Hare, P. D. Townsend, K. Prassides, A. K. Cheetham, H. W. Kroto, and D. R. M. Walton, *Nature*, 1997**, 388**, 52.

24. R. Toledano and D. Mandler, *Chemistry of Materials*, 2010**, 22**, 3943.

25. J. H. Rouse, *Langmuir*, 2005**, 21**, 1055.

26. X. B. Yan, B. K. Tay, and Y. Yang, *Journal of Physical Chemistry B*, 2006**, 110**, 25844.

27. J. Lim, P. Malati, F. Bonet, and B. Dunn, *Journal of the Electrochemical Society*, 2007**, 154**, A140.

28. L. D. Zhu, C. Y. Tian, J. L. Zhai, and R. L. Yang, *Sensors and Actuators B-Chemical*, 2007**, 125**, 254.

29. F. Montilla, M. A. Cotarelo, and E. Morallón, *Journal of Materials Chemistry*, 2009**, 19**, 305.

30. D. Salinas-Torres, F. Montilla, F. Huerta, and E. Morallón, *Electrochimica Acta*, 2011**, 56**, 3620.

31. T. Dobbins, R. Chevious, and Y. Lvov, *Polymers*, 2011**, 3**, 942.

32. R. Esquembre, J. A. Poveda, and C. R. Mateo, *Journal of Physical Chemistry B*, 2009**, 113**, 7534.

33. M. L. Ferrer, R. Esquembre, I. Ortega, C. R. Mateo, and F. del Monte, *Chemistry of Materials*, 2006**, 18**, 554.

34. M. J. O'Connell, S. Sivaram, and S. K. Doorn, *Physical Review B*, 2004**, 69**, 235415.

35. Domingo C. and Santoro G., *Opt.Pura Apl*, 2007**, 40**, 175.

36. M. S. Dresselhaus, G. Dresselhaus, R. Saito, and A. Jorio, *Physics Reports*, 2005**, 409**, 47.

37. R. L. McCreery, *Chemical Reviews*, 2008**, 108**, 2646.

38. D. Salinas-Torres, F. Huerta, F. Montilla, and E. Morallon, *Electrochimica Acta*, 2011**, 56**, 2464.

39. C.G.Zoski, in *Handbook of Electrochemistry; 1ª ed.; Elsevier: Amsterdam*, 2007.